Nigerian Journal of Pharmaceutical and Applied Science Research,12(1): 19-36; March 2023 ISSN: 2971-737X (Print); ISSN: 2971-7388. Available at www.nijophasr.net

Resources Recovery from Mussel shells for the Synthesis and Application of CaO nanoparticles for the Adsorption Remediation of Crystal Violet Contaminated Water

***[1]Anduang O. Odiongenyi, [2]Richard Alexis Ukpe, [1]Iniobong S. Enengedi, [1]Ifiok O. Ekwere, [1]Clement O. Obadimu[1]**

[1]Department of Chemistry, Akwa Ibom State University, Ikot Akpaden, Mkpat Enin LGA, Akwa Ibom State, Nigeria
[2]Department of Chemistry, Federal University, Otuoke, Bayelsa State, Nigeria.,

ABSTRACT

***Background*:** In consideration of the need for effective solid waste management through resource recovery and advanced environmental application techniques, we investigated the potential of mussel shell as a precursor for the synthesis of calcium oxide nanoparticles due to their high content of $CaCO_3$.

Method: Calcium oxide nanoparticles were fabricated from mussel shell wastes (using sol gel method), characterized and applied in the adsorption remediation of crystal violet contaminated water.

***Results*:** The nanoparticles have an average particle size of 2.94 nm, pore volume of 0.254 cc/g and BET surface area of 302 m^2/g. It showed intense FTIR and UV absorption at 1400 cm^{-1} and 238 nm respectively. The band gap and pH at zero charged were also evaluated as 7.1 and 7.2 eV respectively, which indicated that the particles absorb in the UV region and favour the adsorption of crystal violet dye in the basic pH. An increase in temperature decreases the efficiency of the nanoparticles towards the removal of the dye while the removal was favoured by increasing the dye concentration, dosages of the adsorbent, time and ionic strength. The maximum removal efficiency of almost 100% was observed after 1 hour period of contact and at the adsorbate concentration of 100 ppm.

Conclusion: The nanoparticles showed an average of 98% recovery capacity after three times re-used and they are thermally stable above 600 °C.

Keywords: Waste management; resource recovery; sustainable adsorbent; remediation; dye contamination

1. INTRODUCTION

The contamination of the land and the water components of the ecosystem are two major environmental stresses that are receiving global concern regarding the diversities of remediation approaches [1]. Wastes in our environment can assume either of the three states of matter depending on the source. Several domestic and industrial sources have contributed significantly to the current contaminant levels in our society [2]. Commonly encountered toxicity from solid wastes comes from (i) biodegradable wastes that can release leached-out toxic components to the environment, and (ii) those that do not have significant toxicity by themselves but can obstruct the cleaner flow of natural environmental processes and thus constitute secondary pollutants. On the other hand, most industrial effluences are found in liquid or semi-liquid states. The aqueous environment is the major recipient of most toxic contaminants because they tend to dissolve and transport a wide spectrum of contaminants. Dye is one of the most toxic compounds that have been listed among emerging contaminants [3]. Unfortunately, their usefulness in industries such as textile, cosmetics, laboratories, printing, fertilizer, hospital, leather and tanning cannot be overemphasized but their disposal can impact the environment negatively [4]. Crystal violet dye (CV-D) is a basic dye that is highly toxic, especially in aquatic environments. Mirza and Ahmad [5], stated that CV-D interference with the primary productivity of the aquatic environment (i.e. photosynthesis), depletion of the dissolved oxygen content of water, interaction with some metals to form toxic and stable complexes, etc [7-9]. The global researchers' battle to retain the quality of the environment, concerning dye contamination has gained in water can lead to blindness, kidney failure and respiratory disorder.

* Corresponding Author: Email: anduangodiongenyi@aksu.edu.ng.; Phone: +2349073231170

It has also been confirmed that CV-D can penetrate some organisms and render attacks towards mutagenic and carcinogenic attacks [6]. The dye is highly soluble in water and some of the confirmed negative impacts are changes in colour, blockage of light penetration, significant penetration, especially in the development of remediation measures such as adsorption, photocatalysis, dialysis, reverse osmosis, flocculation, filtration, etc [10—14]. Effective waste management involves compromise concerning several factors operating mutually for the achievement or redemption of a cleaner environment at reduced cost and in an eco-friendly manner that is accessible to all. Adsorption is one of the most accessible, cheap and effective methods for the treatment of wastewater, but most adsorbents have been found to exhibit low efficiency, and unsustainable capacity and can easily lose their composition after adsorption [15]. However, nanoparticles have been widely accepted as unique materials that can overcome the present challenges facing the adsorption industries [16-17]. Also, waste Shikuku and Mishra [18] reported a minimum removal efficiency of about 50% for agro wastes that were applied as adsorbents for the removal of some dyes from aqueous solution and concluded that the materials can be improved for better efficiency. A review carried out by Amalina *et al*. [19] reported that a good number of waste biomasses such as sugar cane, seed coat, leaves and other plant parts are effective against the removal of a wider variety of antibiotics. The removal of dyes such as crystal violet dye by some waste biomasses such as wood sawdust [20-21] and bamboo wastes [22]. The removal efficiency exceeding 70% was observed in all the listed processes. Several documented and published works are in strong agreement that the efficiency of an adsorbent generally increases with a decrease in particle size and increased surface area [23-25]. Nanoparticle-based adsorbents are remarkable and generally considered unique because they have high porosity, comparative larger particle size and surface area among other adsorption-related properties [26-27]. Consequently, successes have been recorded in the application of some metal, metal oxides, non-metal based and hybrid nanomaterials as adsorbents for the removal of dyes (including CV-D) from contaminated water [28-30]. However, most of the reported studies have reported ecotoxicological impacts, high cost and inaccessibility of raw materials, elaborate or costly synthetic routes and the challenge of managing the secondary waste product they tend to generate. Therefore, research directed towards the reduction of the highlighted challenges is most desirable for documentation in the scientific literature. The major advantages of using recycling or resource recovery waste management techniques are reduction in the volume of waste, cost saving, environmental friendliness, promotion of accessible raw materials, etc. The achievement expected from the application of biomass-based nanoparticles from waste materials can provide multi-dimensional research benefits if feasible and economical in the management of dye-contaminated water such as CV-D, whose toxicity impacts are well-known and fully established. Therefore, the current study is aimed at recovering $CaCO_3$ from waste mussel shells for further applications in the synthesis of calcium oxide nanoparticles (CaONPs-M) and the removal of CV-D from aqueous medium using the CaONPs-M.

2. MATERIALS AND METHODS

2.1. Sample collection and preparation of CaONPs-M

Mussel shells were purchased from a local market around Oron fishing point. The edible flesh was removed and the shells were washed severally with hot water and dried in an oven to constant weight. The dried samples were crushed into a powdered state using a mechanical blender that was powered by an electric motor. The powder samples were preserved in a desiccator for further application. The first application was the synthesis of CaONPs-M. 20 g of the mussel shell powder was reacted with 2 M HCl solution to convert the $CaCO_3$ content to $CaCl_2$, water and CO_2. The generation and disappearance of the gas were confirmed by effervescence given out as the stirring of the reaction mixture continued. The system was stirred continuously until there was no more release of gas, indicating that only $CaCl_2$ and H_2O were left. The mixture was further reacted with 50% NaOH solution and the NaCl formed was removed by washing the residue severally with water leaving behind, $Ca(OH)_2$ after drying. The dried $Ca(OH)_2$ was calcined in a muffle furnace at 800 °C and the CaONPs-M produced was preserved in a desiccator.

2.2. Characterization of CaONPs-M

The functional groups and vibrations in the CaONPs-M were analysed using an Agilent infrared spectrophotometer (Carry 630 FTIR spectrometer). Zeiss scanning r electron microscopy was used to take the micrograph of the CaONPs-M. BET (Nova 4200e) was used for pore size and pore volume determination through N_2 adsorption study. The adsorption data generated were used to fit several isotherms including Barreett-Joyner-Halenda (BJ-H), multiple BET (M-BET), Langmuir (LN), Dubinin-Ashtakov (D-A), Dubinin-Radushkevich (D-R), Horvath-Kawazoe (HK) and Density theory method (D-F-T). All UV visible measurements were done using Shimadzu (UV-1800 series) spectrophotometer. The thermal stability of the nanomaterials was investigated using Perkin Elmer (model TGA-4000) while pH at zero charges was analysed using the titrimetric method.

2.3. Adsorption removal of CV-D

The adsorption study was conducted using the protocol reported in the literature [31-32]. Parameters investigated were the effect of the period of contact, doses of the adsorbent (i.e. CaONPs-M), concentrations of the adsorbate (i.e. CV-D), pH, ionic strength (using various concentrations of KCl) and temperature. The adsorption study was

done by introducing the test solution into an adsorption flask containing the CaONPs-M as an adsorbent. Depending on the parameter of interest, the control was implemented to obtain results through spectrophotometric measurement at the wavelength, the dye showed maximum absorption. The amount of dye adsorbed was evaluated as the difference between the initial concentration (C_{in}) and the final concentration (C_{out}) while the percentage CV-D adsorbed and the equilibrium amount adsorbed (per unit mass, m given volume, V) were calculated using equations 1 and 2 [33-36]

$$\text{adsorbed} = \frac{C_{in}-C_{out}}{C_{in}} \times \frac{100}{1} \quad (1)$$

$$= \frac{C_{in}-C_{out}}{m} \times \frac{V}{1} \quad (2)$$

In the investigation of the effect of the respective parameters, several values were considered. The parameters included adsorbent dosages, initial dye concentration, ionic strength, time temperature and pH, and various ranges of values were employed. These are 0.1 to 0.5 g, 10 to 100 ppm, 0.01 to 0.10 M, 10 to 60 minutes, 298 to 360 K and 2 to 12 respectively. Also, the investigation was done using fixed values of this constant except for the parameter of interest. For example, the investigation of the effect of pH was carried out using an adsorbent dosage of 0.4 g, temperature of 298 K, initial dye concentration of 100 ppm and contact period of 30 minutes A similar pattern of variations was maintained for the investigation of the effect of the respective parameters.

3. RESULTS AND DISCUSSION

3.1. Characterization of CaONPs-M

Fig. 1a is a 20 μm resolution scanning electron micrograph of the synthesized CaONPs-M, which depicts the appearance of a porous system embedded in the surface. The observation is in support of the literature that nanoparticles are characterized by extraordinal porosity compared to classical materials [37-39]. The CaONPs showed only two major functional groups indicating their relative purity. The observed functional groups were 1395 and 872 cm^{-1}. These groups represent Ca-O vibrations. The pore properties of the CaONPs such as pore diameter, pore size, surface area and surface adsorption energy were evaluated using the Brauner- Emmett- Teller (BET) nitrogen adsorption studies. The data obtained were useful in the fittings of several adsorption isotherms and subsequent evaluation of the listed properties. Adsorption isotherms applied to interpret the nitrogen adsorption results were Barreett-Joyner-Halenda (BJ-H), multiple BET (- M-BET), Langmuir (LN), Dubinin-Ashtakov (D-A), Dubinin-Radushkevich (D-R), Horvath-Kawazoe (HK) and Density theory method (D-F-T). Isotherms-derived pore parameters for the CaONP-M are recorded in Table 1 while Fig. 2 shows plots for the nitrogen adsorption-desorption isotherm, The adsorption-desorption isotherm reveals a different path above a certain pressure, which is approximately 0.5 where the hysteresis starts. This suggests that the adsorption of CV-D occurs through a physical adsorption mechanism [40-41]. The average pore parameters obtained from the different plots are recorded in Table 1. The values indicate that the CaO-NPs-M is a mesoporous material with an average pore diameter of 2.94 nm. Such a class of porosity has been reported by others for CaONPs [42]. However, the Langmuir isotherm shows significantly larger values (942.01 m^2/g) for the surface area compared to the value observed from the M-BET isotherm (302 m^2/g). The observation is not strange but based on generally acceptable literature reference, the Langmuir isotherm can overestimate the pore surface area in the adsorption process that shows a mechanism of physical adsorption and can therefore not be a reliable isotherm for the estimation of the pore properties of this adsorbent of CV-D by the mussel shell based calcium oxide nanoparticles [43]. Other properties were M-BET surface area of 302.24 m^2/g, L-N surface area of 942.01 m^2/g, average micropore volume of 0.314 and characteristics adsorption energy of 4.72 kJ/mol. One of the major characteristics of nanoparticles over other adsorbents is their large surface area to volume ratio which was observed as 1189.92 /m for the synthesized CaONPs-M (based on the M-BET isotherm) . These properties are unique for mesoporous materials and their significance in adsorption has been widely acknowledged [44].

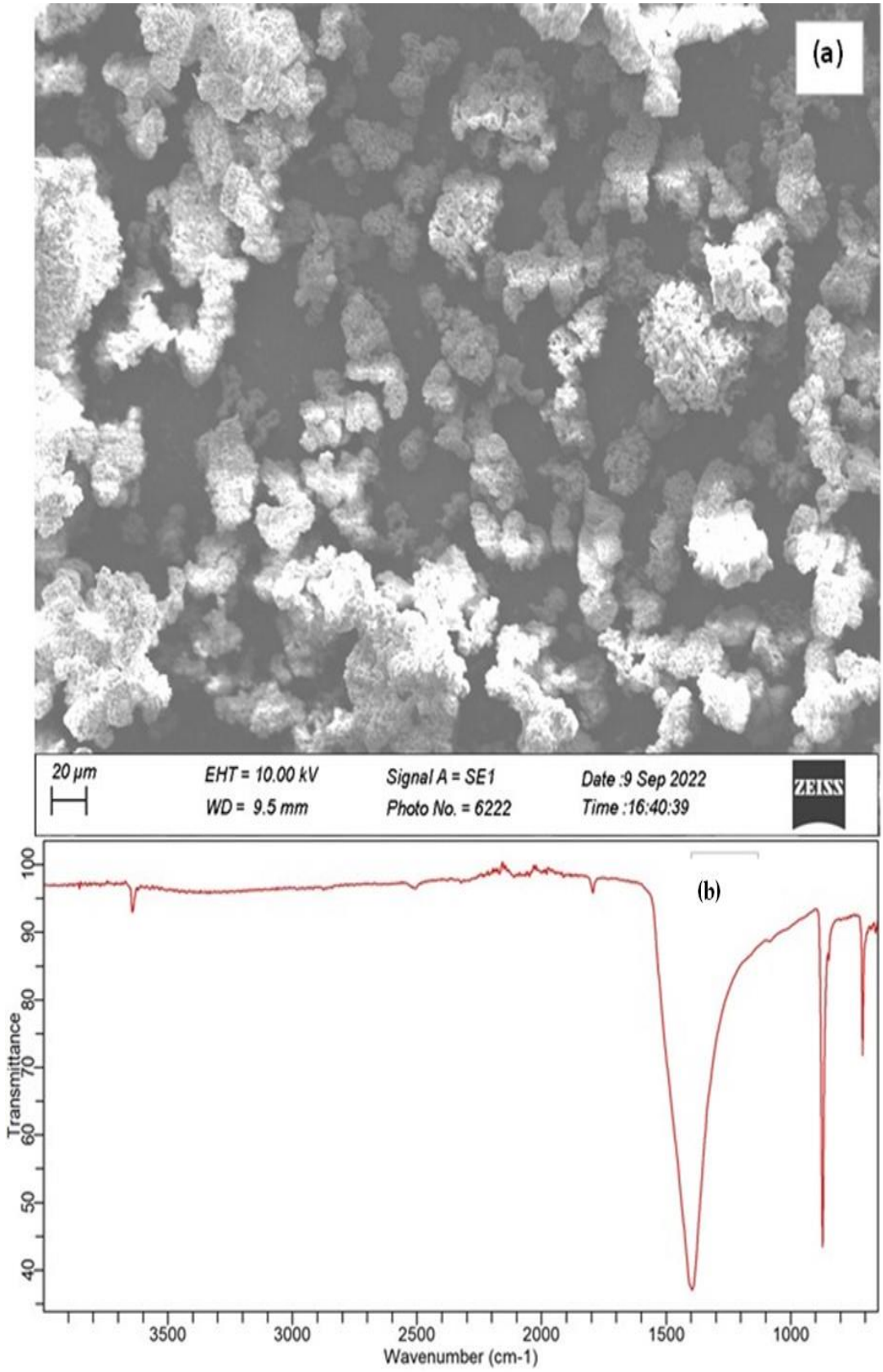

Figure 1. (a) Micrograph from scanning electron microscope of the CaONPs-M (b) FTIR spectrum of the CaONPs-M.

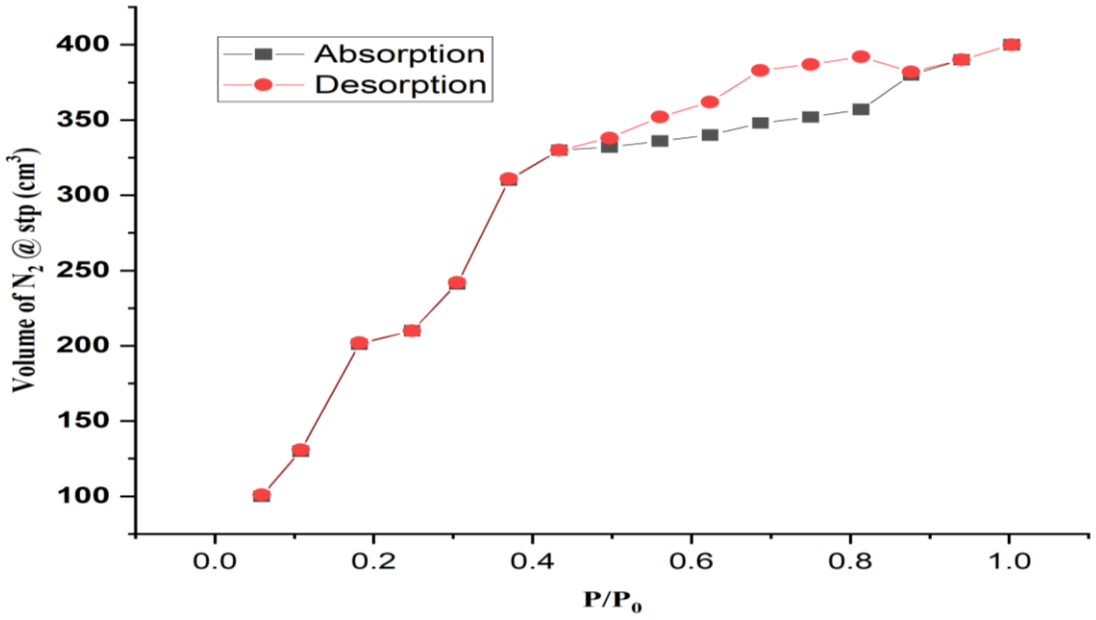

Figure 2. Representative plots for N_2 adsorption study on CaONPs-M based on (a) D-A (b) M-BET

Table 1. Pore parameters for the CaONPs-M.

Pore parameters	Average value	Applied Model
BET Surface area (m^2/g)	302.24	M-BET
L-N surface area (m^2/g)	942.01	L-N
Pore diameter (nm)	2.94	D-A, L-N, DFT, D-R, BJ-H
Pore Volume (cc/g)	0.254	H-K, D-F-T, D-R, D-H, BJ-H
Surface area: Volume (m^{-1})	1189.92	M-BET
Surface area: Volume (m^{-1})	3708.70	M-BET
Micropore volume (cc/g)	0.314	D-A, D-R
Adsorption energy (kJ/mol)	4.72	D-R

Fig. 3 shows the UV-visible spectrum of the CaONPs-M which reveals a maximum wavelength of absorption by the nanoparticles to be 238 nm. The Planck equation (equation 3) can be applied to calculate the energy gap (E_{B-G}) of the CaONPs-M based on equation 3 [44-45],

$$E_{B-G} = \frac{hc}{\lambda_{max}} \quad (3)$$

The Planck constant (h) has a numerical value of 6.6261 x 10^{-34} m^2.kg/s and the speed of light (c) is equal to 2.998 x 10^8 m/s. Consequently, the E_{B-G} of the CaONPs-M is equal to 5.21 eV, which is relatively comparable to those reported for some CaONPs such as 4.9 eV Bhavya *et al*. [49], 3.74 eV [29], 7.1 eV [29], etc. Based on the evaluated E_{B-G} and the λ_{max}, the CaONPs-M absorbs maximally in the UV region and not in the visible region [39]. The thermal stability of the CaONPs-M was investigated using a thermogravimetric and differential thermogravimetric analyzer (TGA/DTA) to analyse the precursor and the results obtained are presented as plots in Fig. 3b. The first weight loss corresponds to a temperature below 180 °C and may be associated with loss of adsorbed water. The second loss occurred between 300 and 400 °C and further descended up to 600 °C but tended to be stable after this temperature. These changes correspond to the destruction of organic content in the mussel shells and finally the formation of the nanoparticles [29]. On the other hand, the DTA plots reveal a major endothermic dip close to 400 °, which can be ascribed to crystalline transformation.

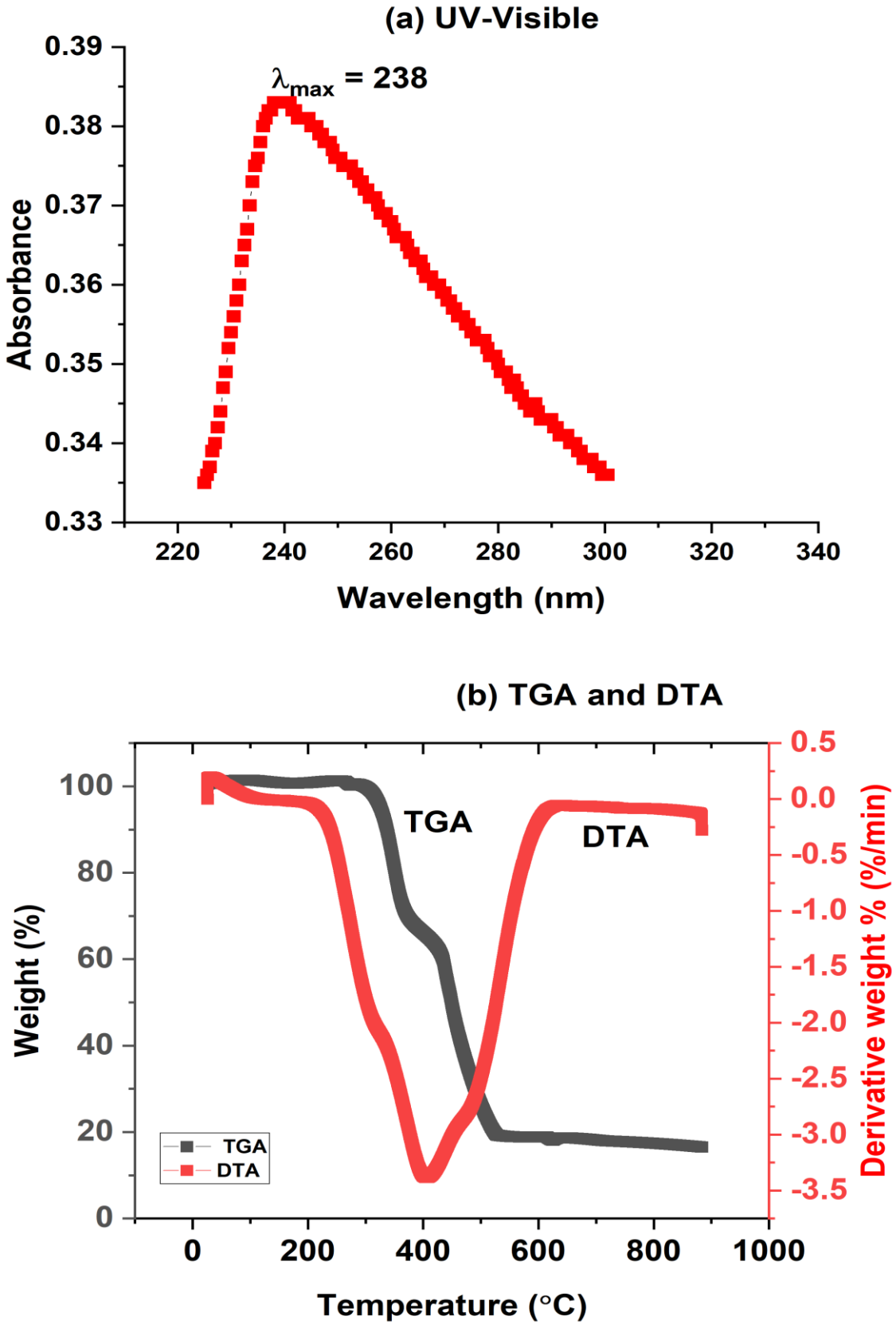

Figure 3: (a) Ulltraviolet-visible spectrum of CaONPs-M (b) TGA and DTA of the conversion of $Ca(OH)_2$ to CaONPs-M.

3.2. Adsorption removal of crystal violet dye by CaONPs-M

The effect of some variables in the alteration of the efficiency of CaONPs for the adsorption of CV-D was investigated concerning initial dye concentration, the mass of the adsorbent, period of contact, time and ionic strength (i.e. [KCl]). Consequently, the contributions of concentration, the mass of adsorbent, ionic strength, period of contact, temperature and pH towards the adsorption process follow the trend shown in Figs. 4a to f

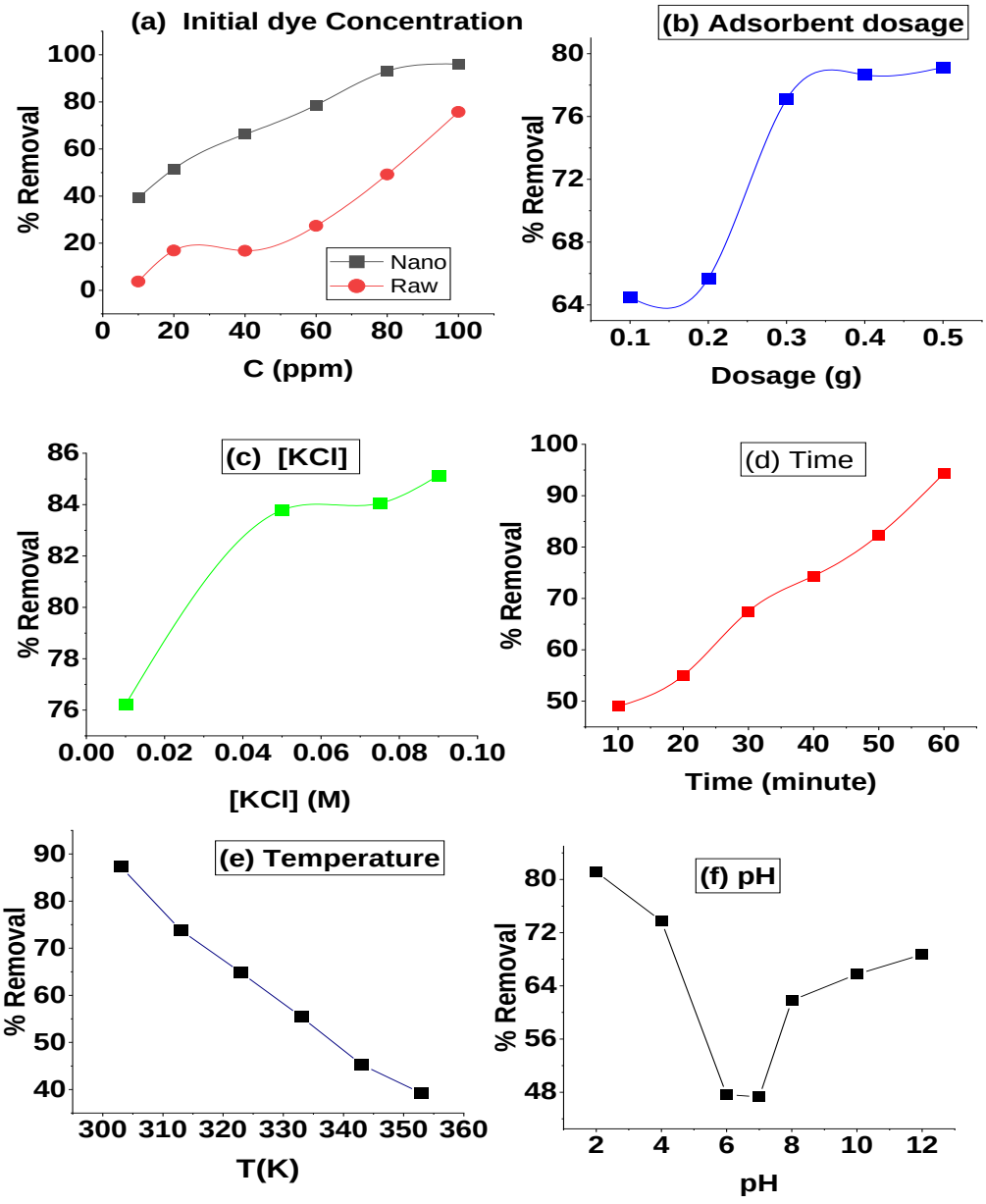

Figure 4. Variation of percentage dye removed with (a) Initial dye concentration (b) Adsorbent dosage (c) [KCl] (d) Time (e) Temperature (f) pH.

An increase in the initial concentration of CV-D resulted in a corresponding increase in the extent of adsorption (Fig.4a) such that at 100 ppm, almost all the CV-D molecules were removed. However, with the crude mussel shell powder, the optimum adsorption was less than 64% which confirms that the transformation to the nanoparticles significantly improved the adsorption capacity of the mussel shell. Generally, an increase in adsorption as a consequence of an increase in concentration is likely due to the corresponding increase in the concentration of the CV-D molecules diffusing to the surface of the CaONPs-M. The consequence is that at higher concentrations of CV-D, the active concentrations of the dye molecules approaching the adsorbent surface will likely, increase the tendency towards adsorption because of the expected rise in the number of available

adsorbate molecules A trend similar to this observation has also been reported by. Cheruiyot *et al*. [50]. The dosages of the adsorbent also showed a primary tendency to increase the extent of adsorption of the CV-D as shown in Fig. 4b. The increment was sharper between 0.2 and 0.4 g, after which the incremental rate was reduced. Also, the initial increment between 0 and 0.2 g was not very sharp. Generally, an increase in adsorbent dosage implies an increase in the active adsorption sites due to the expected increase in surface area. The effect of ionic strength on the adsorption of CV-D was investigated by varying the ionic strength at constant CV-D concentration, fixed mass of adsorbent and fixed temperature. The ionic strength of the solution was varied by introducing different concentrations of KCl to monitor the synergistic or antagonistic effect of the ions on the adsorption of the dye [51]. The results indicated an increase in adsorption as the concentration of the halide ions increased (Fig. 4c). However, the optimum efficiency obtained with 0.1 M KCl (85%) was less than the efficiency observed at CV-D concentration of 100 ppm (99.36%). However, in varying the time, we also observed an optimum efficiency of 99.98% after 1 hour. Ionic strength can alter the surface of the CaONPs-M through interaction with either the surface or with the CV-D to enhance adsorption. Trends similar to the current observation concerning ionic strength) have been reported for some adsorbents that have been used for CV-D [52-53] Variation of adsorption efficiency with time, which showed a proportional relationship in the studied system, is a consequence of an increasing tendency towards the full activation of active adsorbent sites. The reported influence of time on the adsorption of CV-D has been adjudged to have similar trends for some effective nanoparticle adsorbents concerning CV-D [54- 57]. The optimum separation of CV-D from the aqueous solution unto the CaONPs-M was effective at low temperatures. Consequently, the extent of adsorption of the CV-D showed a decrease with an increase in temperature as revealed by Fig. 4e. The efficiency of the CaONPs-M for CV-D adsorption decreased from 90 to 40% between 330 and 360 K. This indicates that the adsorption of the CV-D by CaONPs -M proceeded through a physical adsorption mechanism [59]. The pattern recorded for the adsorption of CV-D concerning temperature does not contradict some published works for the adsorption of CV-D by some nanoparticles [58]. The adsorbent, CaONPs-M displayed a descending capacity for the adsorption of CV-D in acid pH. However in basic pH, an appreciable increase in adsorption with pH was observed (Fig. 4f). To explain this trend, we carried out a titration method for the determination of the pH at zero charges (pHC) for the adsorbed species. As shown in Fig. 5, the PHZC for the CaONPs-M is 7.2 indicating that at pH less than 7.2, the surface of the CaONPs-M is positively charged but negatively charged above 7.2. Consequently, since CV-D is a positively charged dye, its adsorption should be favoured by an alkaline pH (i.e. pH>7.2 (PHZC) as observed in this study (Fig. 4f). This is because a positively charged molecule has a higher tendency to be adsorbed by a negatively charged adsorbent and vice versa.

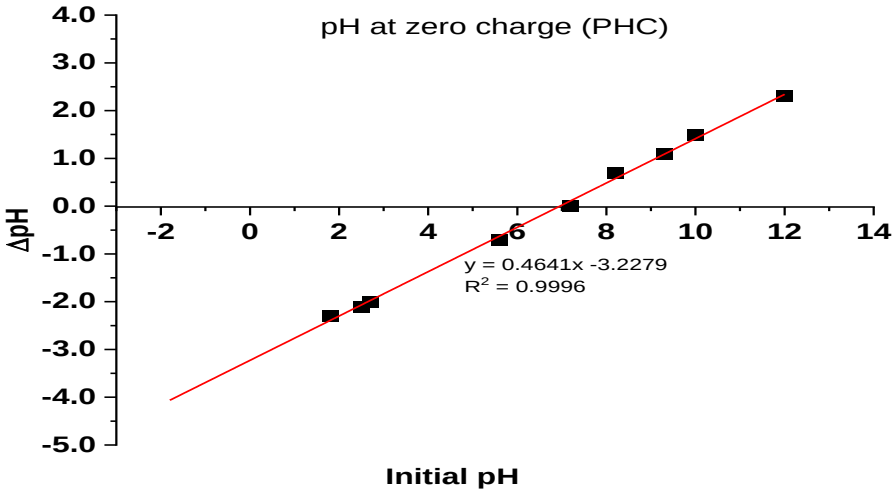

Figure 5. Plots for the change in pH versus initial pH for the determination of PHZC of CaONPs-M.

3.3. Kinetic study on the adsorption of CV-D

Investigated kinetic models were pseudo-first-order (PDFO), pseudo-second (PDSO) order, Elovich (E-L), Weber-Morris (W-M) and liquid film (L-F) kinetic models which are represented by equations 4 to 9 as follows [60-65].

$$\frac{t}{Q_t} = \frac{1}{k_{2ng}}\left(\frac{1}{Q_e^2}\right) + \left(\frac{1}{Q_e}\right)t \qquad (5)$$

$$ln(Q_e - Q_t) = \ln(Q_m) - k_{1st}t \quad (4)$$

$$Q_t = \frac{1}{\beta}\ln(\propto \beta) + \frac{1}{\beta}\ln(t) \quad (6)$$

$$Q_t = k_{M-W}t^{0.5} + I_{M-W} \quad (7)$$

$$-\ln\left(1 - \frac{Q_t}{Q_e}\right) = k_{L-F}t + C_{L-F} \quad (8)$$

$$ln\{-\ln(1 - Q_t)\} = ln(k_{AV-R}) + n_{AV-R}\ln(t) \quad (9)$$

The models presented above were validated based on calculated values of R^2, sum of square error (SSE) , mean square error (MSE) and some theoretical constants with expected ranges. The sum of square error (SSE) and mean square error (MSE) are defined by equations 10 and 11 as follows:

$$SSE = \sum_{1}^{n}(Q_{exp} - Q_{Theor})^2 \quad (10)$$

$$MSE = \Sigma_1^n(Q_{exp} - Q_{Theor})^2 / n \quad (11)$$

Q_{exp} and Q_{Theor} are the experimental and model predicted variables while n is the number of data points used for the evaluation. The PDFO model (equation 4) is founded on the assumption that one adsorbate molecule is adsorbed on one side of the adsorbent and that the extent of adsorption depends on the adsorption capacity of the adsorbent. Both isotherms gave good fitness based on R^2 values (Table 2) but the incorporation of error terms (SSE and MSE) and the comparison of the theoretical rate constants (k_{1st} and k_{2nd}) and the theoretical equilibrium concentration (Q_e) with the experimental values indicated that the adsorption of the CV-D strongly favoured the PDFO. The E-L model gave R^2 fitness parameter of 0.9717 but error terms are not physically significant to validate this model for the adsorption site. Also, the evaluated number of adsorption sites (β) and the rate constants ($\propto$) are. extremely low. Also, the expected chemisorption mechanism proposed by the model is not physically significant, considering the trend obtained from the N_2 adsorption-desorption study and the decreasing trend observed at higher temperatures, both of which confirmed a physical adsorption mechanism. Two basic diffusion models were analysed to evaluate the rate-determining steps concerning intraparticle diffusion (equation 7) and liquid film diffusion (equation 8). Although both models showed a good degree of fitness with lower error values, L-F model gave a zero intercept (i.e. $I_{L-F} = 0$) function unlike the W-M model that has an intercept (I_{M-W}) equal to 2819. Consequently, L-F diffusion is the rate-limiting step for the adsorption of the CV-D by the CaONPs-M. However, the Avrami kinetic model (equation 9 requires that the fitted option is limited by the interaction of the adsorbate on the surface [66]. The fitness of the model is most likely because of the high value of R^2 and the low error values. However, since constant, $n_{AV-R} < 1$, the adsorption is not surface-limited [67]. The evaluated rate constant (k_{AV-R}) is also larger than the average experimental rate constant. From the above analysis and review of kinetic parameters presented in Table 2, the PDFO and the L-F diffusion models best described the adsorption kinetic of CV-D on CaONPs-M surface. Therefore, in Fig. 6a and b, plots showing these two models are presented as representative kinetic plots.

Table 2. Kinetic model parameters for the separation of CV-D from aqueous solution by adsorption onto CaO-NPs-M.

Kinetic model	Plot parameters	Values
PDFO	R^2	0.9958=9
	$k_{1st}(min^{-1})$	1.11009
	$Q_e(mg/g)$	18185.68
	SSE	0.00000071
	MSE	0.0000001902
PDSO	R^2	0.95801
	$k_{2nd}(min^{-1})$	1.3000
	$Q_e(mg/g)$	2378.69
	SSE	1.3556×10^{-7}
	MSE	3.3889×10^{-8}

E-L	R^2	0.9717
	β	0.0001429+
	$\ln(\propto \beta)$	-10108.25
	SSE	1077564.93
	MSE	389188.31
W-M	R^2	0.9610
	$k_{W-M}(min^{-1})$	2016.80
	I_{W-B}	2819.13
	SSE	2759601
	MSE	6899900
L-F	R^2	0.937
	$k_{L-F}(min^{-1})$	0.0350
	C_{L-F}	0.0000
	SSE	0.00397
	MSE	0.00132
AV-R	R^2	0.9871
	n_{AVR}	0.3007
	$k_{AV-R}(min^{-1})$	4.82
	SSE	0.00231
	MSE	0.000007702

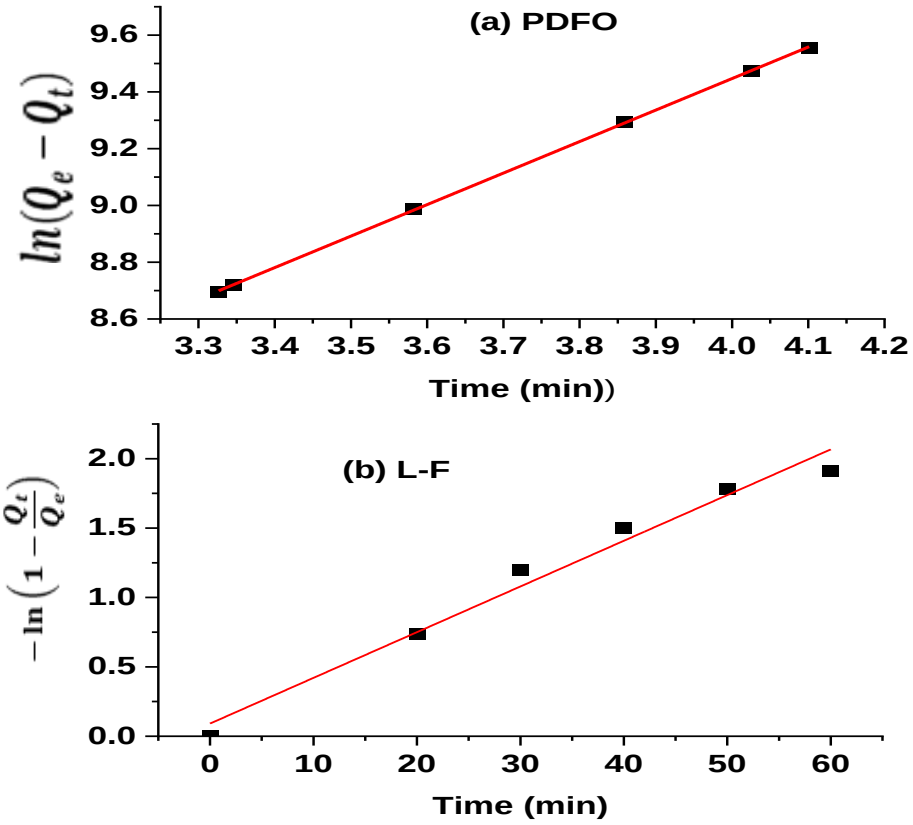

Figure 6. (a) Pseudo-first-order and (b) Liquid film diffusion plots for the adsorption of CV-D by CaONPs-M.

The Langmuir (L-N) isotherm was verified and confirmed by the linearity of a plot of $\frac{C_e}{Q_e}$ versus C_e which is consistent with equation 12 [68],

$$\frac{C_e}{Q_e} = C_e \frac{1}{Q_{max}} + \frac{1}{Q_{max} k_{L-N}} \quad (12)$$

The plot (Fig. 7a} gave interesting results and seems to show the high linearity parameters. These included R^2 value (0.9995), lowest SSE and MSE values recorded in Table 3 while the error bar in the plots correlates with the data point more than other isotherms that fitted the adsorption of the investigated dye by CaONPs-M. The L-N maximum adsorption capacity deduced from the plot (i.e. 9646.92 mg/g) is in strong agreement with the experimental Q_{max} even at the advantage of a better slope error reference estimator. The intercept also had a significantly lower error (1.3664×10^{-4}), which also made it a good estimator of the L-N adsorption equilibrium constant, evaluated as 0.07052 L/mol. However, although the L-N plot describes best fitness, the extremely high values of the Langmuir adsorption capacity are physically insignificant and may not translate to the real situation. As stated before, where the mechanism of physical adsorption prevails, the Langmuir isotherm is not applicable, irrespective of the fitness of the model.

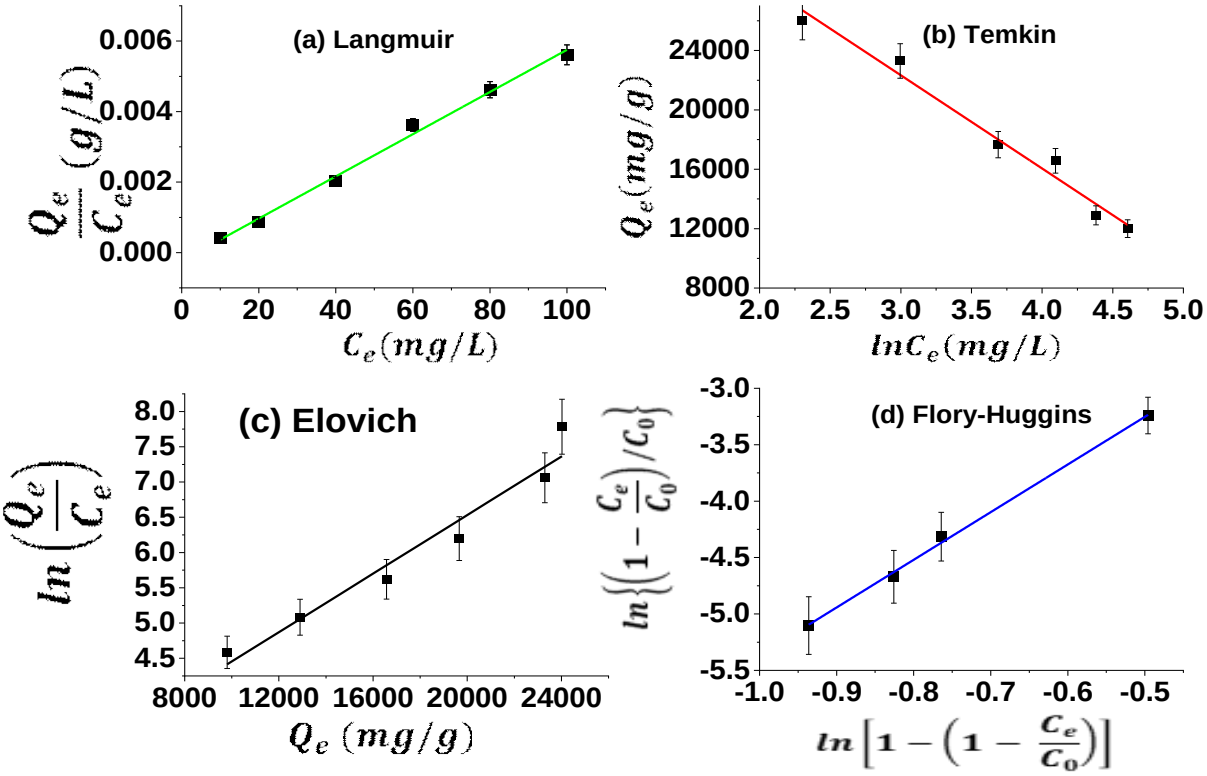

Figure 7. Adsorption isotherm for the adsorption of CV-D by CaONPs-M based on (a) Langmuir (b) Temkin (c) Elovich and (d) Flory Huggins models.

The Temkin (T-N) model showed the least degree of fitness (R^2 = 0.9002) and the highest set of errors. The model is represented according to equation 13 [69],

$$Q_e = B_{T-N} ln C_e k_{T-N} \quad (13)$$

The T-N constant, B_{T-N} equates the adsorption energy, which was obtained (as -6089.51 J/nol) from the slope of the plot of Q_e against lnC_e (Fig. 7b). A consideration of the assumption of T-N model implies a physical adsorption mechanism with negative interaction parameters. The Temkin equilibrium constant displayed a numerical value of 0.00138 L/mol.

The Elovich model explains the expectation of a proportional and exponential increase in the number of adsorption sites with adsorption. As shown in equation 14 [70-71],

$$\frac{Q_e}{Q_{max}} = k_{E-L} C_e \frac{Q_e}{Q_{max}} \quad (14)$$

The linear form of the above equation is more applicable in terms of a logarithm function as follows:

$$ln\left(\frac{Q_e}{C_e}\right) = ln(k_{E-L}Q_{max}) - \frac{Q_e}{Q_{max}} \quad (15)$$

The suitability of the Elovich isotherm for the adsorption of the dye was validated by the linear plot obtained for $ln\left(\frac{Q_e}{C_e}\right)$ versus $ln\left(\frac{Q_e}{C_e}\right)$ as shown in Fig 7c. Information on the E-L plot (Table 3) supports good fitness based on the magnitude of R^2, SSE and MSE respectively. Consequently, the Q_{max} was evaluated as 481.44 mg/g while k_{E-L} is evaluated as 0.003817 L/mol.

The Flory Huggins isotherm can be established if a linear plot of $\boldsymbol{ln\left\{\left(1-\frac{C_e}{C_0}\right)/C_0\right\}}$ **versus** $\boldsymbol{\left[1-\left(1-\frac{C_e}{C_0}\right)\right]}$ gives better fitness to interpret slope and intercept as n_{F-H} and lnk_{F-H} respectively [72]. The model (equation 16) has two major constants, namely, nk_{F-H} representing the number of dye molecules that occupy a given adsorption site while lnk_{F-H} is the Flory-Huggins adsorption equilibrium constant of adsorption

$$\boldsymbol{ln\left\{\left(1-\frac{C_e}{C_0}\right)/C_0\right\} = lnk_{F-H} + n_{F-H}ln\left[1-\left(1-\frac{C_e}{C_0}\right)\right]} \quad (16)$$

The plot (Fig. 7d) reveals $nk_{F-H} = 4$, suggesting the occupancy of four molecules per adsorption site, which is not uncommon for multiple molecular layer adsorption systems where the mechanism of physical adsorption is significant. Based on the isotherms discussed above, the Flory Huggins model seems to explain the adsorption of the CV-D by CaNPs-M better than other models. The fitness of Flory-Huggins isotherm for the adsorption of CV-D has also been observed by other authors for the adsorption of crystal violet dye [73].

Table 3. Parameters of the described adsorption isotherms.

Lang	Parameter	value
	$Slope$	$1.0366 \times 10^{-4} \pm 1.368 \times 10^{-4}$
	$Intercept$	$-2.3094 \pm 1.3664 \times 10^{-4}$
	R^2	0.9995
	$Q_{max}\ (mg/g)$	9646.92
	SSE	1.2335×10^{-7}
	MSE	3.0838×10^{-8}
T-N	$Slope$	-6089.514 ± 1066.42
	$Intercept$	40105.62 ± 984.23
	R_T(J/mol)	6089.51
	k_{T-N} (L/mol)	0.00138
	R^2	0.9007
	SSE	12.441
	MSE	9.8740
F-H	$Slope$	4.224 ± 0.1295
	$Intercept$	-1.4048 ± 0.0928
	n_{F-H}	4
	lnk_{F-H}	1.4048
	R^2	0.9981
	SSE	0.0473
	MSE	0.0473
Elovich	$Slope$	$2.0767 \times 10^{-4} \pm 2.281 \times 10^{-3}$
	$Intercept$	2.3777 ± 0.4209
	$Q_{max\ (mg/g)}$	481.33
	R^2	0.9540
	k_{E-L}	0.00382
	SSE	
	MSE	0.0842

3.4. Regeneration of the adsorbent

Regeneration of the adsorbent was carried out by washing the used adsorbent with distilled water severally, followed by drying and re-application for adsorption study. The recovery efficiency was calculated based on the ratio of the measured percentage CV-D adsorbed before and after re-used of CaONPs-M (equation 17)

$$Recovery\ efficiency = \frac{\%\ removal\ by\ CaONP - M}{\%\ removal\ by\ the\ re-used\ CaONPs - M} \times \frac{100}{1} \quad (17)$$

The recovery experiments were conducted to reflect the initial concentrations of CV-D earlier declared and three trial experiments were conducted (Fig.8). The results presented in Fig. 8 indicate that the CaONPs-M is recyclable and can retain more than 98% average efficiency after three trials.

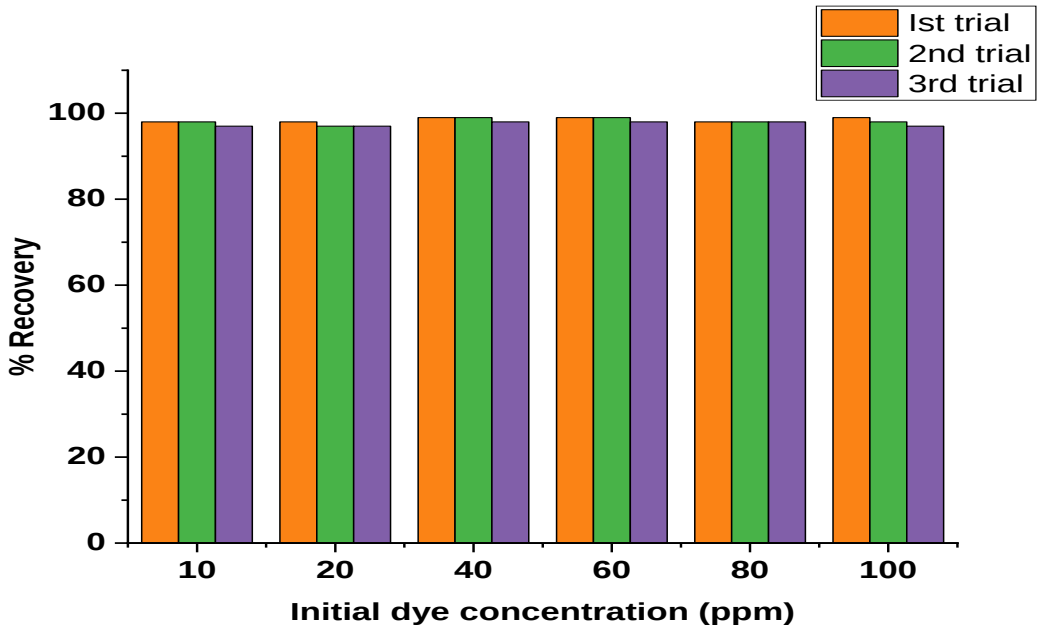

Figure 8. Bar charts representing the recovery efficiency of CaONPs-M for CV-D after three trials at various concentrations.

A further investigation of the changes in the chemical nature of the adsorbent after re-use was done through the FTIR analysis of the used and washed CaONPs-M, which indicated no change in functional groups but less than 2% drop in absorption intensity.

4. CONCLUSION

The present study was conducted to recover a sustainable adsorbent from waste mussel shells for the remediation of crystal violet-contaminated water. The results and findings from the study led to the following conclusions,

(i) Mussel shell is an excellent source of $CaCO_3$ and hence a precursor for the synthesis of calcium oxide nanoparticles.

(ii) The synthesized CaONPs-M belongs to the mesoporous class with unique porosity and excessively large surface area to volume ratio.

(iii) The CaONPs-M synthesized is stable at higher temperatures (> 600 °) and retains up to 98% of its adsorption efficiency even after three trials.

(iv) Optimum efficiency of the CaOBPs-M can best be controlled by concentration, time, pH, ionic strength, temperature and pH.

Acknowledgment

The authors acknowledge the support of Prof. Nnabuk Okon Eddy in providing laboratory space for all analyses and for the sponsorship through the Tertiary Education Trust Fund.

Funding

The research was fully sponsored by the Tertiary Education Trust Fund of Nigeria (TETFUND) under the National Research Grant (2020) through Prof. Nnabuk Okon Eddy of the Department of Chemistry, University of Nigeria, Nsukka.

Conflict of Interest

The authors have no relevant financial or non-financial interests to disclose

Contribution of the Authors

The work was designed by Dr. Anduang Odiongenyi and Dr. Richard Ukpe. The initial draft was written by the two authors while all the authors were involved in the benchwork.

REFERENCES

[1] Shao, P.; Yin, H., Li, Y.; Cai, Y., Yan, C.; Yuan, Y. 'Dang, Z.. Remediation of Cu and As contaminated water and soil utilizing biochar supported layered double hydroxide: Mechanisms and soil environment altering. Journal of Environmental Sciences, 2023, 26, 275-286, https://doi.org/10.1016/j.jes.2022.05.025.

[2] Chen, W.; Chen, Y.; Shu, Y.; He, Y.; Wei, J. Characterization of solid, liquid and gaseous products from waste printed circuit board pyrolysis. Journal of Cleaner Production, 2021, 313, https://doi.org/10.1016/j.jclepro.2021.127881.

[3] Slama, H. B.; Chenari Bouket, A.; Pourhassan, Z.; Alenezi, F. N.; Silini, A.; Cherif-Silini, H.; Oszako; T.; Luptakova; L.; Golińska, P.; Belbahri, L. . Diversity of synthetic dyes from textile industries, discharge impacts and treatment Methods. *Appl. Sci., 2021*, 11, 6255, https://doi.org/10.3390/app11146255.

[4] Eddy, N. O.; Ukpe, R. A.; Ameh, P.; Ogbodo, R.; Garg, R.; Garg, R. (2022)a. Theoretical and experimental studies on photocatalytic removal of methylene blue (MetB) from aqueous solution using oyster shell synthesized CaO nanoparticles (CaONP-O). Environmental Science and Pollution Research, https://doi.org/10.1007/s11356-022-22747-w

[5] Mirza, A.; Ahmad, R. An efficient sequestration of toxic crystal violet dye from aqueous solution by Alginate/Pectin nanocomposite: A novel and ecofriendly adsorbent. Groundwater for Sustainable Development, 2020, 11,https://doi.org/10.1016/j.gsd.2020.100373.

[6] Oloo, C.; M., Onyari, J. M.; Wanyonyi, W. C.; Wabomba, J. N.; Muinde, V. M. (2020). Adsorptive removal of hazardous crystal violet dye form aqueous solution using Rhizophora mucronata stem-barks: Equilibrium and kinetics studies. Environmental Chemistry and Ecotoxicology, 2020, 2, 64-72.https://doi.org/10.1016/j.enceco.2020.05.001.

[7] Ahmad, R.; Ansari, K. (2020). Polyacrylamide-Grafted *Actinidia deliciosa* peels powder (PGADP) for the sequestration of crystal violet dye: isotherms, kinetics and thermodynamic studies. *Appl Water Sci*, *2*, 10, 195, https://doi.org/10.1007/s13201-020-01263-7.

[8] Gomaa, H.; Abd El-Monaem, E. M.; Eltaweil, A. S.; Omer, A. M. Efficient removal of noxious methylene blue and crystal violet dyes at neutral conditions by reusable montmorillonite/$NiFe_2O_4$@amine-functionalized chitosan composite. *Scientific Report*, 2022, 12, 15499, https://doi.org/10.1038/s41598-022-19570-1.

[9] Chwastowski, J.; Staro, P.; Pieta, E.; Paluszkiewicz, C. Bioremediation of Crystal Violet by Organic Matter and Assessment of Antimicrobial Properties of the Obtained Product. Sustainability 2023, 15, 67. https://doi.org/10.3390/ su15010067.

[10] Eddy, N. O., Odiongenyi, A. O., Garg, R., Ukpe, R. A., Garg, R., El Nemir, A., Ngwu, C. M. and Okop, I. J. (2023). Quantum and experimental investigation of the application of *Crassostrea gasar* (mangrove oyster) shell–based CaO nanoparticles as adsorbent and photocatalyst for the removal of procaine penicillin from aqueous solution. *Environmental Science and Pollution Research*, 2023, doi:10.1007/s11356-023-26868-8.

[11] Eddy, N. O., Garg, R., Garg, R., Eze, S. I., Ogoko, E. C., Kelle, H. I., Ukpe, R. A., Ogbodo, R. and Chijoke, F. Sol-gel synthesis, computational chemistry, and applications of Cao nanoparticles for the remediation of methyl orange contaminated water. Advances in Nano Research, 2023, https://doi.org/10.12989/anr.2023.15.1.000

[11] Odiongenyi, A. O. and Afangide, N. R.. Adsorption and thermodynamic studies on the removal of congo red dye from aqueous solution by alumina and nano-alumina. Communication in Physical Sciences, 2019, 4(1): 1-7.

[12] Salunkhe, B. and Schuman, T. P. Super-Adsorbent hydrogels for removal of methylene blue from aqueous solution: dye adsorption isotherms, kinetics, and thermodynamic properties. *Macromol* , 2021,1, 256-275. https://doi.org/10.3390/macromol1040018

[13] Teng, W.; Liu, S.; Zhang, X.; Zhang, F.; Yang, X.; Xu, M.; Hou, J. (2023). Reliability treatment of silicon in oilfield wastewater by electrocoagulation. *Water, 2023, 15, 206,* https://doi.org/10.3390/w15010206.,

[14] Yuthawong, V.; Thongnueahaa, C.; Phungsai, P. Changes in optical properties and molecular composition of dissolved organic matter and formation of disinfection by-products during conventional water treatment processes. Environmenta; Science and Water Research technology,2023, 9, 161-175, https://doi.org/10.1039/D2EW00423B.

[15] Odoemelam, S. A., Emeh, N. U. and Eddy, N. O. Experimental and computational Chemistry studies on the removal of methylene blue and malachite green dyes from aqueous solution by neem (*Azadiractha indica*) leaves. Journal of Taibah University of Science, 12(3, 2018, 255–265, doi.org/10.1080/16583655.2018.1465725.

[16] Garg, R.; Garg, R.; Eddy, N. O.; Almohana, A. I.; Fahad, S.; Khan, M. A.; Hong, S. H. Biosynthesized silica-based zinc oxide nanocomposites for the sequestration of heavy metal ions from aqueous solutions. *Journal of King Saud University*-Science, 2022, https://doi.org/10.1016/j.jksus.2022.101996.

[17] Rápó, E.; Tonk S. Factors Affecting Synthetic Dye Adsorption; Desorption Studies: A Review of Results from the Last Five Years (2017-2021). Molecules. 2021, 26, 17, 5419. doi: 10.3390/molecules26175419.

[18] Shikuku, V. O. and Mishra, T. Adsorption isotherm modeling for methylene blue removal onto magnetic kaolinite clay: a comparison of two-parameter isotherms. *Applied Water Science* (2021), 11, 103, https://doi.org/10.1007/s13201-021-01440-2.

[19] Amalina, F., Abd Razak, A. S., Krishnan, S., Zularisam, A. W. and Nasrullah, M. Dyes removal from textile wastewater by agricultural waste as an absorbent – A review. Cleaner Waste Systems, 2022, 3, https://doi.org/10.1016/j.clwas.2022.100051.

[20] Akpanudo, N. W. and Chibuzo, O. U.Musanga cecropioides Sawdust as an Adsorbent for the Removal of Methylene Blue from Aqueous Solution. *Communications in Physical Sciences*, 2020, 5(3): 262-370.

[21] Khine, E. E., Koncz-Horvath, D., Kristaly, F., Ferenczi, T., Karacs, G., Baumli, P. and Kaptay, G. Synthesis and characterization of calcium oxide nanoparticles for CO_2 capture. *J Nanopart Res* 2022, 24, 139, https://doi.org/10.1007/s11051-022-05518-z

[22] Keri, A.; Sap, A.; Ungoa, D.; Sebok, D.; Csapo, E.; Konya, Z.; Galbacs, G. Porosity determination of nano- and sub-micron particles by single particle inductively coupled plasma mass spectrometry. Journal of Analytical Atomic Spectrum, 2020, 35, 1139, doi: 10.1039/d0ja00020e rsc.li/jaas

[23] Bensacia, N.; Fechete, I.; Boutemak, K.; Kettab, A. Mesoporous materials for adsorption of heavy metals from wastewater. In: Lichtfouse, E., Muthu, S.S., Khadir, A. (eds) Inorganic-organic composites for water and wastewater treatment. Environmental Footprints and Eco-design of Products and Processes. Springer, Singapore, 2022,. https://doi.org/10.1007/978-981-16-5916-4_8.

[24] Bhavya, C.; Yogendra, K.; Mahadevan, K. M.; Madhusudhana, N. Synthesis of calcium oxide nanoparticles and its mortality study on fresh water fish *Cyprinus carpio*. IOSR Journal of Environmental Science, Toxicology and Food Technology, 2016, 10, 12, 55-60, doi: 10.9790/2402-1012015560.

[25] Gandhi, N.; Shruthi, Y.; Sirisha, G.; Anusha, C. R. Facile and Eco-Friendly method for synthesis of calcium oxide (CaO) nanoparticles and its potential application in agriculture. Haya Saudi J Life Sci,2021, 6,5,: 89-103.

[26] Alavi, M. A.; Morsali, A. Ultrasonic-assisted synthesis of $Ca(OH)_2$ and CaO nanostructures, Journal of Experimental Nanoscience, 2010, 5:2, 93-105, doi: 10.1080/17458080903305616.

[27]. Osuntokun, J.; Onwudiwe, D. C.; Ebenso, E. E. Aqueous extract of broccoli mediated synthesis of CaO nanoparticles and its application in the photocatalytic degradation of bromocrescol green. IET Nanobiotechnology, 2018, 12, 7, 888-894. doi: 10.1049/iet-nbt.2017.0277.

[28] Marquis, G.; Ramasamy, B.; Banwarilal, S.; Munusamy, A. P. Evaluation of antibacterial activity of plant mediated CaO nanoparticles using Cissus quadrangularis extract, Journal of Photochemistry and Photobiology B: Biology, 2016, 155, 28-33, ,https://doi.org/10.1016/j.jphotobiol.2015.12.013.

[29] Silva, V. C.; Araújo, M. E. B.; Rodrigues, A .M.; Vitorino, M.d. B. C.; Cartaxo, J. M.; Menezes, R. R.; Neves, G. A. Adsorption behavior of crystal violet and congo red dyes on heat-treated brazilian palygorskite: kinetic, isothermal and thermodynamic studies. Materials, 2021, 14, 19, 5688; **https://doi.org/10.3390/ma14195688**

[30] Mirghiasi, Z.; Bakhtiari, F.; Darezereshki, E.; Esmaeilzadeh, E. Preparation and characterization of CaO nanoparticles from Ca(OH)2 by direct thermal decomposition method", *J. Ind. Eng. Chem.*,2014, 20, 1, 113–117. https://doi.org/10.1016/j.jiec.2013.04.018.

[31] Odiongenyi, A. O. Influence of sol gel conversion on the adsorption capacity of crab shell for the removal of crystal violet from aqueous solution. *Communication in Physical Science*, 2022, 8(1):121-127.

[32] Odiongenyi, A. O. Removal of ethyl violet dye from aqueous solution by graphite dust and nano graphene oxide synthesized from graphite dust. Communication in Physical Sciences, 4(2):103-109.

[33] Alobi, N. O. and Chibuzo, O.. Wood sawdust as adsorbent for the reomoval of direct (DR) dye from aqueous solution. Communication in Physical Sciences, 2019, 4(1-2): 160-166.

[34] Eddy, N. O., Ibok, U. J., Garg, R., Garg, R. Falak, A. I., Amin, M., Mustafa, F., Egilmez, M. and. Galal, A. M. A brief review on fruit and vegetable extracts as corrosion inhibitors in acidic environments of steel in acidic environment. *Molecules*, 2022, 27, 2991. https:// doi.org/10.3390/molecules27092991.

.[35]Eddy, N. O., Odoemelam, S. A. And Ibiam E. Ethanol extract of *Occimium gratissimum* as a green corrosion inhibitor for mild steel in H_2SO_4. *Green Chemistry Letters and* Review, 2010, 3,3, 165-172. DOI: 10.1080/17518251003636428. https://doi.org/10.1016/j.rechem.2022.100290.

[36] Eddy, N. O., Ukpe, R. A., Ameh, P., Ogbodo, R., Garg, R. and Garg, R. Theoretical and experimental studies on photocatalytic removal of methylene blue (MetB) from aqueous solution using oyster shell synthesized CaO nanoparticles (CaONP-O). Environmental Science and Pollution Research, 2022b, https://doi.org/10.1007/s11356-022-22747-w

[37] El Kassimi, A.; Achour, Y.; El Himri, M.; Laamari, R.; El Haddad, M. Removal of two cationic dyes from aqueous solutions by adsorption onto local clay: experimental and theoretical study using DFT method, International Journal of Environmental Analytical Chemistry, 2021, DOI: 10.1080/03067319.2021.1873306.

[38] Odiongenyi, A. O. Utilization of *Musa cecropiodesi* woood saw dust for the removal of dispersed yellow (DY) dye from aqueous solution. *Communication in Physical Sciences* 5(3): 270-280.

[39] Odiongenyi, A. O. Influence of sol gel conversion on the adsorption capacity of crab shell for the removal of crystal violet from aqueous solution**.** Communication in Physical Sciences, 2022, 8, 1, 121-127.

[40] Morsi,, R. E. and Mohamed, R. S. Nanostructured mesoporous silica: influence of the preparation conditions on the physical-surface properties for efficient organic dye uptake.R. Soc. open sci.(2018), 5: 172021. http://dx.doi.org/10.1098/rsos.172021

[41] Rizzi, F., Castaldo, R., Latronico, T., Lasala, P., Gentile, G., Lavorgna, M., Striccoli, M., Agostiano, A., Comparelli, R., Depalo, N., Curri, M. L. and Fanizza, E. High surface area mesoporous silica nanoparticles with tunable size in the sub-micrometer regime: insights on the size and porosity control mechanisms. *Molecules,2021, 26*, 4247, https://doi.org/10.3390/molecules26144247.

[42] Ogoko, E. C., Kelle, H. I., Akintola, O. and Eddy, N. O. Experimental and theoretical investigation of *Crassostrea* gigas (gigas) shells based CaO nanoparticles as a photocatalyst for the degradation of bromocresol green dye (BCGD) in an aqueous solution. *Biomass Conversion and Biorefinery*. 2023, https://doi.org/10.1007/s13399-023-03742-8 .

[44] Bensacia, N.; Fechete, I.; Boutemak, K.; Kettab, A. Mesoporous materials for adsorption of heavy metals from wastewater. In: Lichtfouse, E., Muthu, S.S., Khadir, A. (eds) Inorganic-organic composites for water and wastewater treatment. Environmental Footprints and Eco-design of Products and Processes. Springer, Singapore, 2022,. https://doi.org/10.1007/978-981-16-5916-4_8.

[44] Bhavya, C.; Yogendra, K.; Mahadevan, K. M.; Madhusudhana, N. Synthesis of calcium oxide nanoparticles and its mortality study on fresh water fish *Cyprinus carpio*. IOSR Journal of Environmental Science, Toxicology and Food Technology, 2016, 10, 12, 55-60, doi: 10.9790/2402-1012015560.

[45] Odoemelam, S. A., Oji, E. O., Eddy, N. O., Garg, R., Garg, R., Islam, S., Khan, M. A., Khan, N. A. and Zahmatkesh, S. Zinc oxide nanoparticles adsorb emerging pollutants (glyphosate pesticide) from aqueous solution. *Environmental Monitoring and Assessment*, https://doi.org/10.1007/s10661-023-11255-0.

[50] Alavi, M. A.; Morsali, A. Ultrasonic-assisted synthesis of $Ca(OH)_2$ and CaO nanostructures, Journal of Experimental Nanoscience, 2010, 5:2, 93-105, doi: 10.1080/17458080903305616.

[51] Cheruiyot, G. K., Wanyonyi, W. C., Kiplimo, J. J. and Maina, E. N. Adsorption of toxic crystal violet dye using coffee husks: Equilibrium, kinetics and thermodynamics study. Scientific African (2009), 5, https://doi.org/10.1016/j.sciaf.2019.e00116.

[52] Eddy, N. O. and Ita, B. I. (2011). Theoretical and experimental studies on the inhibition potentials of aromatic oxaldehydes for the corrosion of mild steel in 0.1 M HCl. *Journal of Molecular Modeling* 17: 633-647. DOI:10.1007/s00894-010-0749.

[53] Mannu, A.; Di Pietro, M. E.; Mele, A. Band-gap energies of choline chloride and triphenylmethylphosphoniumbromide-based systems. Molecules, 2020, 25;25(7):1495. doi: 10.3390/molecules25071495.

[54] Lim, L., Priyantha, N., Cheng, H. H. and Zaidi, N. A. H. M. Parkia speciosa (Petai) pod as a potential low-cost adsorbent for the removal of toxic crystal violet dye. Scientia Bruneiana, 2018, doi:10.46537/scibru.v15i0.26.

Mannu, A., Di Pietro, M. E. and Mele, A. Band-gap energies of choline chloride and triphenylmethylphosphoniumbromide-based systems. Molecules, 2020, 25,25(7):1495. doi: 10.3390/molecules25071495.

[55] Foroutan, R.; Peighambardoust, S. J.; Peighambardoust, S. H.; Pateiro, M.; Lorenzo, J. M. Adsorption of Crystal Violet Dye Using Activated Carbon of Lemon Wood and Activated Carbon/Fe_3O_4 Magnetic Nanocomposite from Aqueous Solutions: A Kinetic, Equilibrium and Thermodynamic Study. *Molecules,2021, 26*, 2241. https://doi.org/10.3390/molecules26082241.

[56] Sun, P.; Hui, C.; Azim Khan, R.; Du, J.; Zhang, O.; Zhao, Y. Efficient removal of crystal violet using Fe_3O_4-coated biochar: the role of the Fe_3O_4 nanoparticles and modeling study their adsorption behavior. *Scientific Report*, 2025, 12638, https://doi.org/10.1038/srep12638

[57] Samrot, A. V.; Ali, H. H.; Selvarani, J. A.; Faradjeva, E.; Prakash, R. P.; Kumar, S. Adsorption efficiency of chemically synthesized superparamagnetic iron oxide nanoparticles (SPIONs) on crystal violet dye, Current Research in Green and Sustainable Chemistry, 2021, 4, https://doi.org/10.1016/j.crgsc.2021.100066

[58] Al-Ajji, M. and Al-Ghouti, M. A. Novel insights into the nanoadsorption mechanisms of crystal violet using nano-hazelnut shell from aqueous solution. Journal of Water Process Engineering, 2021, 44, https://doi.org/10.1016/j.jwpe.2021.102354.

[59] Eddy, N. O., Odoemelam, S. A. and Ibiam E (2010). Ethanol extract of *Occimium gratissimum* as a green corrosion inhibitor for mild steel in H_2SO_4. *Green Chemistry Letters and Review*, 3(3): 165-172. DOI: 10.1080/17518251003636428,

[60] Benjelloun, M.; Miyah, Y.; Evrendilek, G. A.; Zerrouq, F.; Lairini, S. Recent advances in adsorption kinetic models:their application to dye types. Arabian Journal of Chemistry, 2021, 14, 4, https://doi.org/10.1016/j.arabjc.2021.103031.

[61] Brandani, S. Kinetics of liquid phase batch adsorption experiments. *Adsorption*, 2021, **27**, 353–368, https://doi.org/10.1007/s10450-020-00258-9.

[62] Hambisa, A. A.; Regasa, M. B.; Ejigu, H. G.; Senbeto, C. B. Adsorption studies of methyl orange dye removal from aqueous solution using Anchote peel-based agricultural waste adsorbent. *Applied Water Science*, 2020, 13, https://doi.org/10.1007/s13201-022-01832-y.

[63] Kostoglou, M.; Karapantsios, T. D. Why Is the Linearized Form of Pseudo-Second Order Adsorption Kinetic Model So Successful in Fitting Batch Adsorption Experimental Data? Colloids Interfaces, 2022, 6, 55. https://doi.org/10.3390/ colloids604005.

[64] Modwi, A.; Elamin, M. R.; Idriss, H.; Elamin, N. Y.; Adam, F.A.; Albadri, A.E.; Abdulkhair, B. Y. Excellent Adsorption of Dyes via $MgTiO_3$@g-C_3N_4 Nanohybrid: Construction, Description and Adsorption Mechanism. *Inorganics* **2022**, *10*, 210. https://doi.org/10.3390/inorganics10110210.

[65]. Yousaf, A.; Salman, M.; Rehman, R.; Farooq, U. Detoxification of toxic cations Pb(II) and Cd(II) from liquid phase by employing *Pennisetum glaucum* biowaste: a kinetic investigation, International Journal of Phytoremediation,2022, 24, 2, 110-117, DOI: 10.1080/15226514.2021.1926913.

[66] Georgin, J.; da Silva Marques, B.; da Silveira Salla, J.; Foletto, E. L.; Allasia, D.; Dotto, G. L.. Removal of Procion Red dye from colored effluents using H2SO4-/HNO3-treated avocado shells (Persea americana) as adsorbent. Environ Sci Pollut Res, 201,8 25, 6429–6442. https://doi.org/10.1007/s11356-017-0975-1.

[67] Ahmad, A. A.; Din, A. T. M.; Yahaya, N. K .E.; Khasri, A.; Ahmad, M. A. Adsorption of basic green 4 onto gasified Glyricidia sepium woodchip based activated carbon: Optimization, characterization, batch and column study. Arabian Journal of Chemistry, 2020, 13, 6887–6903. https://doi.org/10.1016/j.arabjc.2020.07.002.

[68] Ozcan, C. and Gurel, E. N. l, L. A comparison for the removal of two different textile dyes by raw *Helianthus annuus* L. seed shells. *Int. J. Environ. Sci. Technol.* 2023, https://doi.org/10.1007/s13762-022-04729-0.

[69] Mustapha, O. R.; Osobamiro, T. M.; Sanyaolu, M. O.; Alabi, S. M. Adsorption study of Methylene blue dye: an effluents from local textile industry using *Pennisteum pupureum* (elephant grass), International Journal of Phytoremediation, 2023, DOI: 10.1080/15226514.2022.2158781.

[70] Debord, J.; Harel, M.; Bollinger, J.; Chu, K. H. The Elovich isotherm equation: Back to the roots and new developments, Chemical Engineering Science,2022, 262, https://doi.org/10.1016/j.ces.2022.118012.

[71] Edet, U. A.; Ifelebuegu, A. O. Kinetics, isotherms, and thermodynamic modeling of the adsorption of phosphates from model wastewater using recycled brick waste. *Processes, 2020, 8,:* 665. https://doi.org/10.3390/pr8060665.

[72] Salunkhe, B. and Schuman, T. P. Super-Adsorbent hydrogels for removal of methylene blue from aqueous solution: dye adsorption isotherms, kinetics, and thermodynamic properties. *Macromol* , 2021,1, 256-275. https://doi.org/10.3390/macromol1040018

[73] Chwastowski, J., Staro, P., Pieta, E. and Paluszkiewicz, C. Bioremediation of Crystal Violet by Organic Matter and Assessment of Antimicrobial Properties of the Obtained Product. Sustainability 2023, 15, 67. https://doi.org/10.3390/ su15010067.